

Search for the Higgs boson decaying into 4 leptons via ZZ^* and the reconstruction of electrons in the CMS experiment at LHC.

Mykhailo Dalchenko

May 9, 2011

1 Introduction

The Standard Model of particle physics is a model concerning the electromagnetic, weak, and strong nuclear interactions, which mediate the dynamics of the known subatomic particles. Developed throughout the early and middle 20th century, the current formulation was finalized in the mid 1970s upon experimental confirmation of the existence of quarks. Since then, discoveries of the bottom quark (1977), the top quark (1995) and the tau neutrino (2000) have given credence to the Standard Model. Because of its success in explaining a wide variety of experimental results, the Standard Model is sometimes regarded as a theory of almost everything. Nevertheless, there are still unexplained phenomena such as, for example, the generation of the fermion masses and hierarchy problem.

A cornerstone of the SM is the mechanism of spontaneous electroweak symmetry breaking (EWSB) proposed forty years ago by Higgs, F. Englert and R. Brout (see [1], [2]) to generate the weak vector boson masses in a way that is minimal and respects the requirements of renormalizability [3] and unitarity. An $SU(2)$ doublet of complex scalar fields is introduced and its neutral component develops a non-zero vacuum expectation value. As a consequence, the electroweak $SU(2)_L \otimes U(1)_Y$ symmetry is spontaneously broken to the electromagnetic $U(1)_Q$ symmetry. Three of the four degrees of freedom of the doublet scalar field are absorbed by the W^\pm and Z bosons to form their longitudinal polarizations and to acquire masses. The fermion masses are generated through a Yukawa interaction with the same scalar field and its conjugate field. The remaining degree of freedom corresponds to a scalar particle, the Higgs boson. The discovery of this new type of particle is unanimously considered to be of profound importance. Direct searches for the SM Higgs particle at the LEP e^+e^- collider have lead to a lower mass bound of $m_H > 114.4 \text{ GeV}/c^2$ (95% C.L.) [5]. Ongoing direct searches at the Tevatron $p\bar{p}$ collider by the D0 and CDF experiments set constraints on the production cross-section for a SM-like Higgs boson in a mass range extending up to about $200 \text{ GeV}/c^2$, and the range $158 < m_H < 173 \text{ GeV}/c^2$ was excluded (95% C.L.) [6]. A consistency fit including all the measured electroweak observables which are sensitive to the existence of a Higgs boson through virtual processes, favors a low mass with $m_H < \sim 182 \text{ GeV}/c^2$.

One of the most promising road towards a discovery at the Large Hadron Collider (LHC) of the Higgs boson postulated in the SM is via single production followed by a cascade decay into charged leptons, $H \rightarrow ZZ^{(*)} \rightarrow l^+l^-l^+l^-$. The single Higgs boson production benefits from a high cross-section, with values of about $15 \times 10^3 \text{ fb}$ at $m_H = 130 \text{ GeV}/c^2$ and decreasing monotonically to about $2.5 \times 10^3 \text{ fb}$ around $m_H = 300 \text{ GeV}/c^2$ (see Fig. 1). The production cross-section is dominated ($\gtrsim 80\%$) over this mass range by gluon-gluon fusion processes via triangular loops involving heavy quark (mostly the top quark) flavours. The branching ratio for the $H \rightarrow ZZ^{(*)}$ decay in the SM is sizeable for any m_H value above $130 \text{ GeV}/c^2$ as shown in Fig. 1. The Z bosons have a 10% probability to yield a pair of charged leptons. Thus, the decay chain $H \rightarrow ZZ^{(*)} \rightarrow l^+l^-l^+l^-$ (in short $H \rightarrow 4l$) offers a possibly significant and very clean and simple multi-lepton final state signature for the SM Higgs boson at the LHC. Ultimately, the channel can provide a precise determination of the Higgs boson mass and production cross-section. The anti-correlation of the Z spin projections in the $H \rightarrow ZZ$ decay and the polarization of each Z boson can be used to constrain, and eventually determine, the spin and CP quantum numbers of the Higgs resonance. Furthermore, the $ZZ^{(*)}$ and $WW^{(*)}$ decay modes are related via $SU(2)$ and the combination of channels could allow for cancellation of some systematic uncertainties

in a determination of the Higgs coupling. But first and foremost is the necessity to be best prepared for a discovery at the LHC. This requires the development of algorithms for accurate reconstruction of the leptons in the detector.

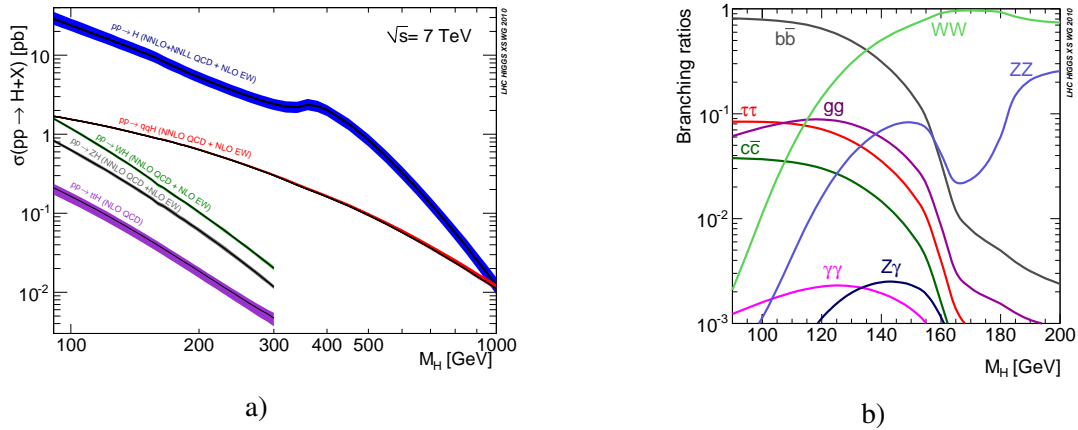


Figure 1: Production cross-sections and branching fractions of the Higgs boson [4].

2 Experimental framework

The Large Hadron Collider was built by the European Organization for Nuclear Research (CERN) with the intention of testing various predictions of high-energy physics, including testing for the existence of the hypothesized Higgs boson and of the large family of new particles predicted by supersymmetry. It was built in collaboration with over 10,000 scientists and engineers from over 100 countries, as well as hundreds of universities and laboratories. LHC is a proton-proton collider contained in a circular tunnel, with a circumference of 27 kilometers, at a depth ranging from 50 to 175 meters underground. The four main experiments are all run by international collaborations.

There are two large experiments at the LHC, ATLAS (A Toroidal LHC ApparatuS) and CMS (Compact Muon Solenoid), which can satisfy all conditions needed for the Higgs boson search. CMS is designed as a general-purpose detector, capable of studying many aspects of proton collisions at 14 TeV, the center-of-mass energy of the LHC particle accelerator. The scheme of the CMS is shown on the Fig. 2. It contains subsystems which are designed to measure the energy and momentum of photons, electrons, muons, and hadrons. The innermost layer is a silicon-based tracker. Surrounding it is a scintillating crystal electromagnetic calorimeter, which is itself surrounded with a sampling calorimeter for hadrons. The tracker and the calorimetry are compact enough to fit inside the CM Solenoid which generates a powerful magnetic field of 4 T. Outside the magnet are the large muon detectors, which are inside the return yoke of the magnet.

I have chosen CMS for my future work because I have already some experience of working at the CMS group at National Science Center "Kharkiv Institute for Physics and Technology". My previous topic of research was the studying of the angular distributions of the multi-lepton Higgs boson decays from the phenomenological side, and now I want to complete this search from the experimental point of view. The choice of the laboratory for the pre-thesis internship and PhD thesis in the future was motivated by the topic of proposed research and its participation in the CMS experiment.

There are approximately 3,600 people from 183 scientific institutes, representing 38 countries from the CMS collaboration who built and now operate the detector. One of the laboratories participating in this experiment is the Laboratoire Leprince-Ringuet (LLR).

The LLR is a joint research unit (UMR 7638) of the Institut National de Physique Nucléaire et de Physique des Particules (IN2P3) of Centre National de la Recherche Scientifique (CNRS) and École Polytechnique. It is located on the site of the Ecole Polytechnique in Palaiseau (91). From 1974 to 2001 it was known as the Laboratory of Nuclear Physics of High Energies (LPNHE-X). The laboratory's research program focuses on particle physics and astrophysics.

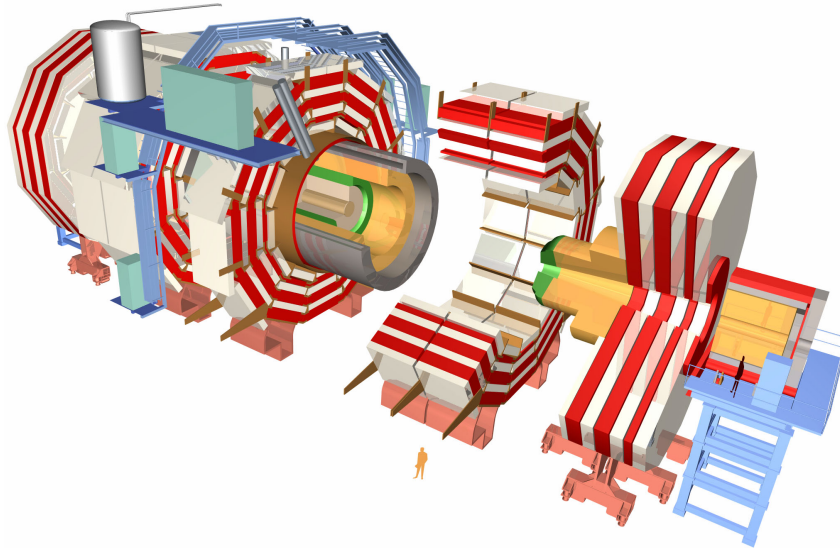


Figure 2: The overview of the CMS detector

The particle physics part of research activity related to the study of electroweak interactions (ALEPH, H1, CMS, T2K), CP-symmetry violation (BaBar), and quark-gluon plasma (NA50, Phenix). They take place at accelerators at CERN (Geneva, Switzerland), DESY (Hamburg, Germany), SLAC (Stanford, California, USA), RHIC (Brookhaven, New York, USA) and JPARC (Tokai, Japan).

Since 1990, a program of astrophysics, high energy gamma astronomy, has been undertaken, first at Mount Whipple (Arizona, USA) and the Themis site in the Pyrenees (CELESTE and CAT), currently in Namibia (HESS) and space (satellite FERMI).

These experiments require detectors of large size and complexity, they take place in three phases, design, construction and operation of the detector. The first two involve the assistance of technical major in mechanical, electronic and information technology. The laboratory has a group at each experiment. An administrative service ensures the smooth running of the whole.

The CMS group at LLR consists of ~ 25 researchers, which 13 Permanent and 6 PhD. The team involved in the CMS experiment since the design of detectors. The main topics of activity are design and operation of the CMS Electro-Magnetic Calorimeter (ECAL) and trigger optimization as well as electron reconstruction, data acquisition and analysis. One of the most important areas of work in the group is the search for the Higgs boson (in the frames of the Standard Model or beyond) decaying to the multi-lepton final states.

3 Electron Reconstruction in the CMS

The reconstruction of electrons in CMS uses information from the pixel detector, the inner tracker and the electromagnetic calorimetry (ECAL). A detailed description of the CMS detector can be found elsewhere [7]. Some of the relevant characteristics of the main detectors used for electron reconstruction are described below.

3.1 CMS tracker and ECAL detectors

The CMS tracker is a cylindrical detector of 5.5 m in length and 1.1 m in radius. It is equipped with silicon pixel detectors (66 M channels) for the innermost part (for radii $R < 15\text{ cm}$ and for $|z| < 50\text{ cm}$) and silicon strip detectors (2.8 M channels) for the outer layers ($R < 110\text{ cm}$, $|z| < 275\text{ cm}$). The pixel detectors provide in general 2 or 3 hits per track, each with a three-dimensional precision of about $10\ \mu\text{m}$ in the transverse plane ($R\phi$) and $15\ \mu\text{m}$ in z . The strip detectors can provide up to 14 hits per track, with a two-dimensional precision ranging from $10\ \mu\text{m}$ to $60\ \mu\text{m}$ in $R\phi$. Some of the silicon strip layers are double-sided to provide a longitudinal measurement with a similar accuracy. The tracker acceptance for

a minimum of 5 collected hits extends up to pseudorapidities η of about $|\eta| < 2.5$. The efficiency for collecting 2 hits in the pixel detector drops from close to 100% at $|\eta| \simeq 2.1$ to below 70% at $|\eta| \simeq 2.5$.

The material thickness in the tracker volume to be traversed by electrons and photons before reaching the ECAL varies strongly with η . It amounts to about $0.4X_0$ at central pseudorapidities ($\eta = 0$), increases to $\simeq 2X_0$ towards the ECAL barrel/endcap transition, and falls back to about $1.3X_0$ at $|\eta| = 2.5$. One can see the sketch of the CMS detector on the Fig. 3

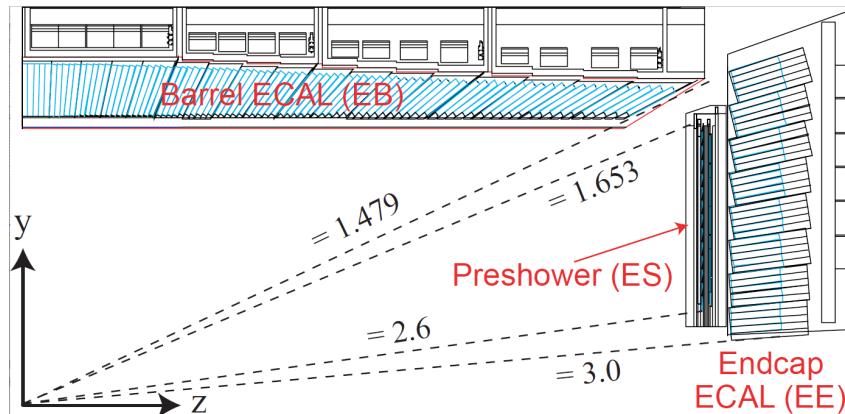


Figure 3: The view of one quarter of the CMS detector

The CMS ECAL [7] is made of $PbWO_4$ crystals, a transparent material denser ($8.3 g/cm^3$) than iron, with a radiation length X_0 of $0.89 cm$ and a Moliere radius R_M of $2.19 cm$. The ECAL is composed of a barrel covering $|\eta| \lesssim 1.48$ and two endcaps covering $1.48 \lesssim |\eta| \lesssim 3.0$. The barrel is made of 61200 trapezoidal and quasiprojective crystals of approximately $1.3 \times R_M$ in lateral size and about $25.8X_0$ in depth. The barrel inner radius is of $124 cm$. Viewed from the nominal interaction vertex, the individual crystals appear tilted (off-pointing) by about 3° both in polar and azimuthal angles, and the granularity is about $\Delta\eta \times \Delta\phi = 0.0175 \times 0.0175 rad$. The barrel is divided in two halves, each made of 18 supermodules containing 1700 crystals. Each supermodule is composed of four modules. The endcaps consist of two detectors, a preshower device followed by $PbWO_4$ calorimetry. The preshower is made of silicon strips placed in a $19 cm$ sandwich of materials including about $2.3X_0$ of Pb absorber. The preshower covers inner radii from $45 cm$ to $123 cm$, corresponding to the range $1.6 < |\eta| < 2.6$. Each endcap calorimeter is made of 7324 rectangular and quasi-projective crystals of approximately $1.3 \times R_M$ in lateral size and about $24.7X_0$ in depth. The crystal front faces are aligned in the (x, y) plane but, as for the barrel, the crystal axes are off-pointing from the nominal vertex in the polar angle by about 3° . The CMS inner tracking and ECAL detectors are immersed in a $4 T$ magnetic field parallel to the z axis.

The tracks in CMS are reconstructed with a Kalman Filter (KF) approach, assuming that the charged particle is a muon. For muons, the multiple Coulomb scattering is the dominant effect on the particle while crossing material, and its impact is modeled by Gaussian fluctuations. This approach is not suitable for electrons where the dominant effect is the highly non-Gaussian Bremsstrahlung emission. Fig. 4 shows for example the distribution of the fraction of the initial energy radiated by electrons before reaching the ECAL, for electrons of 10, 30 and 50 GeV. Such a distribution is the result of the convolution of the bremsstrahlung spectrum, the finite path to reach the ECAL and the finite initial energy of the electrons. About 35% of the electrons radiate more than 70% of their initial energy before reaching the ECAL. In about 10% of the cases, more than 95% of the initial energy is radiated.

3.2 Electron Clustering and Seeding

The electromagnetic showers initiated by electrons (or photons) deposit their energy in several crystals of the ECAL. Most of the energy from a single electron (or photon) reaching the ECAL is collected in a small number of crystals. The original seeding strategy was designed and optimised for isolated electrons with a large transverse momentum (p_T). It starts from the ECAL clusters, and is hereafter called the ECAL-driven approach. It relies on the property that the position of the barycentre of all the ECAL energy deposits, resulting from an electron, does not depend on the Bremsstrahlung photon emission.

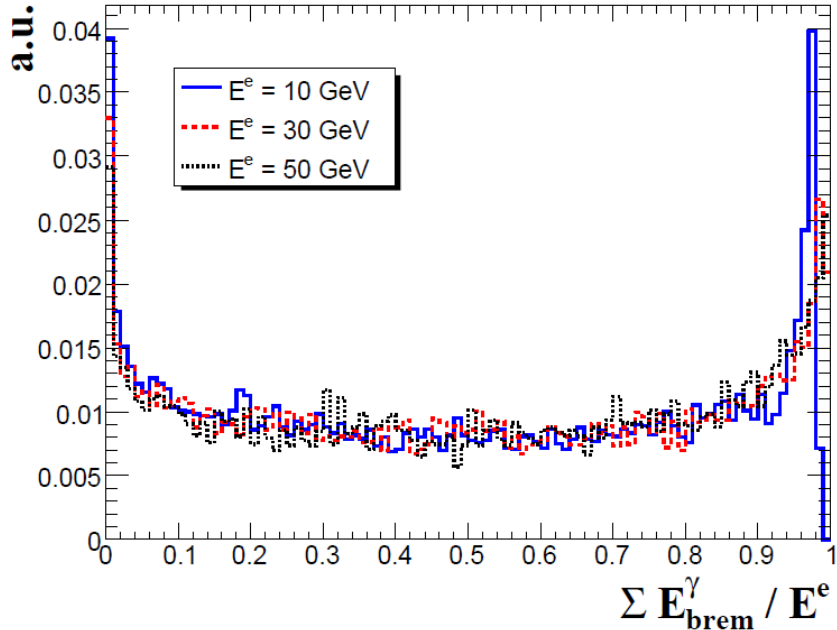


Figure 4: Distribution of the fraction, $\Sigma E_{brem}^\gamma / E^e$, of the generated electron energy (E^e) radiated as bremsstrahlung photons (E_{brem}^γ) for electrons of 10, 30 and 50 GeV. The true emission of bremsstrahlung photons has been integrated up to a radius corresponding to the ECAL inner radius.

The general track seeds found to match the predicted hit positions are selected. The performance of this method depends on the ability to gather into one “super-cluster” all the Bremsstrahlung photon and electron energy deposits. To do so, all the energy deposits in the ECAL in a large region along ϕ are collected around the crystal with the local energy maximum. In most of the cases, this algorithm allows the electrons from converted Bremsstrahlung photons to be recovered. Only the super-clusters with a transverse energy exceeding 4 GeV are considered.

There are two basic clustering algorithms, “Hybrid” and “multi5x5” used for electrons in the ECAL barrel and endcaps respectively. The “Hybrid” algorithm allows creation of the super-clusters obtained by grouping dominoes within a ϕ window around the starting crystal up to a maximum extension of 0.3 rad in both directions. The “multi5x5” first collects the energy deposited in the crystals within 5×5 matrices. Then super-clusters are created by combining such clusters whose position lies within a ϕ road of extension 0.3 rad in ϕ , as for the barrel case.

This procedure is well suited for isolated and high p_T electrons but not for non-isolated or low- p_T electrons. There are several problems for electrons within a jet. Indeed, the super-cluster position and energy can be biased by the contribution of overlapping particles. Moreover, because of the high track multiplicity, the backward propagation from the super-cluster can be compatible with several track seeds originating from other charged particles. To limit the number of fake seeds inside jets, the ECAL-driven seeding requires that the ratio between the HCAL and ECAL energy deposit is smaller than 0.15. This causes some limitation in the detection efficiency but the fake seed rate is kept under control. For the low- p_T electrons the spread in ϕ , due to the Bremsstrahlung photons, can be so wide that the super-cluster cannot include all the deposits.

In order to properly handle with low- p_T and electrons inside the jets the particle-flow reconstruction method was developed. In the particle-flow, seeding starts from the tracker and therefore called “tracker-driven” seeding strategy. A GSF (Gaussian Sum Filter)/KF track is linked to a given cluster if the extrapolated position from the outermost tracker measurement in the calorimeter is within the boundaries of one of the cells constituting the cluster. For each tracker layer, where the material is mainly localised, a Bremsstrahlung photon emission is sought by computing a straight-line extrapolation, tangent to the track, up to the ECAL, preshower and HCAL. Then it creates a super-cluster that contains within itself all the clusters satisfying this link condition. To reduce the charged hadron contamination, the ECAL clusters already matched with a KF track are discarded from this procedure. Moreover, to limit the

background due to neutral particles, the distance in η between the cluster and the extrapolation should be smaller than 0.015. The procedure in the case of an electron emitting a single Bremsstrahlung photon, is illustrated in Fig. 5 where the GSF track, the extrapolated track tangents, and the ECAL clusters are visible.

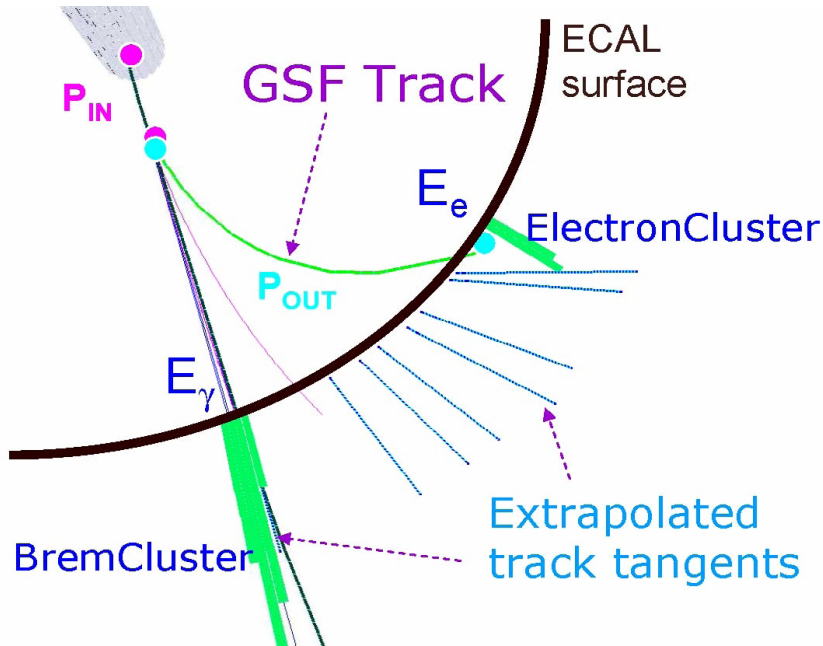


Figure 5: Electron representation in a transverse view.

3.3 Tracking

In the case of energetic Bremsstrahlung photon emission, causing a kink in the electron trajectory, the pattern recognition is often not able to follow the electron path. In contrast, when the photon energy is moderate, the pattern recognition can succeed in collecting all the hits, but the quality of the track fit can be poor.

Therefore, a dedicated electron track reconstruction had to be developed [8]. First step is to take the compatible hits in the tracker layers, then perform an extrapolation, using a Bethe-Heitler modeling of the electron losses and a GSF in the forward fit. In order to preserve efficiency and to follow electron trajectories in case of bremsstrahlung emission, a very loose χ^2 compatibility is required in the building steps of the electron tracking. The combinatorics is limited by requiring at most 5 candidate trajectories at each tracker layer and at most one layer with missing hit. Finally, in order to reduce the probability to connect a primary electron to a leg from a photon conversion, a high χ^2 penalty is used in the cases of missing hit.

The GSF leads to multi-component trajectory states for each measurement point, with weights for each component describing the associated probability. Although more information is available, one usually considers two combinations in order to estimate the track momentum parameters at each measurement point: the weighted mean of the components (so called "mean") and highest weight component (so called "mode"). While the mean estimate is in average less biased, it has been shown that the mode estimate is more precise for low radiating tracks. On the contrary, tracks that have been subject to important bremsstrahlung losses have their reconstructed momentum underestimated, creating a typical low momentum tail.

The GSF tracking runs on the merged collection of seeds and the resulting GSF tracks are used by both the standard and the particle-flow electron reconstruction algorithms. As explained in Sec. 1, electrons traversing the tracker detector emit a non-negligible amount of Bremsstrahlung photons which afterwards can convert into electron-positron pairs. Bremsstrahlung photons converting in the pixel detector can generate additional electron seeds both for the ECAL-driven and tracker-driven algorithms, while only the tracker-driven seeding is sensitive to the Bremsstrahlung photons converting further in

the tracker. The tracker-driven seeding indeed uses all high-purity tracks, included those produced in the fourth and fifth iterations. These tracks are not required to have their first hit close to the interaction point. Those additional seeds imply that more than one GSF track per electron can be reconstructed occasionally.

3.4 Preselection

Electron candidates are built from the reconstruction of GSF tracks and their associated super-clusters. In the case of electrons with ECAL-driven seeds, the associated super-cluster is simply the super-cluster that initiated the seed reconstruction. For the cases of electrons with seeds only found by the tracker-driven seeding algorithm, a tracker-driven bremsstrahlung recovery algorithm and identification of the "electron cluster" is used. This tracker driven algorithm runs on all GSF tracks to produce super-clusters by grouping together particle flow clusters which are matched with presumed "photon" lines, tangent to the electron trajectory at any of the tracker measurement layers. The electron cluster, defined as the cluster matched with the outermost track state, is finally added to the super-cluster. This procedure leads to a new collection of super-clusters that are used to build the electron candidates for the cases of electrons with tracker-driven only seeds. In addition, several track-cluster matching observables are combined, together with the track p_T and η , using a boosted decision tree (BDT) to obtain a global identification variable hereafter called " mva ". The observables used include pure tracking observables based on the GSF track and the comparison with the track as obtained from the standard (MIP) track reconstruction, observables relative to the energy matching between the track and the calorimeter, the bremsstrahlung photon cluster pattern analysis and the cluster shape of the electron cluster. The mva , together with the super-cluster built in this procedure, are made available for all GSF tracks. Electron candidates, formed by the association of a GSF track and its associated super-cluster, are then preselected using available track-cluster matching observables in order to reduce the rate of jets faking electrons. The preselection is made very loose so to efficiently reconstruct electrons and satisfy a large number of possible analyses.

For electrons that have an ECAL driven seed, the following cuts have been already applied at the seeding level:

- $E_T > 4 \text{ GeV}/c$, where E_T is the supercluster transverse energy,
- $H/E < 0.15$, where H is the energy deposited in the HCAL towers in a cone of radius $\Delta R = 0.15$ centered on the electromagnetic supercluster position and E is the energy of the electromagnetic supercluster,
- $|\Delta\eta_{in}^{extrap}| = |\eta_{sc} - \eta_{in}^{extrap}| < 0.02$, where η_{sc} is the energy weighted position in η of the supercluster and η_{in}^{extrap} is the η coordinate of the position of closest approach to the super-cluster position, extrapolating from the innermost track position and direction,
- $|\Delta\phi_{in}^{extrap}| = |\phi_{sc} - \phi_{in}^{extrap}| < 0.02$, where ϕ_{sc} is the energy weighted position in ϕ of the supercluster and ϕ_{in}^{extrap} is the ϕ coordinate of the position of closest approach to the super-cluster position, extrapolating from the innermost track position and direction.

For the cases of electrons with seed only found by the tracker driven algorithm, the global identification variable mva as obtained from the BDT is used. Electron candidates in these cases are required to satisfy:

- $mva > -0.4$, where mva is the output of BDT.

4 Momentum determination and E-p combination

On order to take all advantages of the track momentum estimation in particular in the low energy region and/or in the ECAL crack regions, the electron momentum magnitude is obtained from the combination of the ECAL and the tracker measurements. Starting from the energy as obtained from the super-cluster after ECAL level corrections (from hereafter labeled E), the momentum magnitude can be further refined

by splitting electrons into different classes and performing class dependent corrections. Following [11], the electron classification is based on the observed number of clusters inside the super-cluster in the ECAL and on the measured bremsstrahlung fraction by the tracker. The classification has been further refined and the electron classes are defined as follows:

golden , or low bremsstrahlung electrons with a reconstructed track well matching the supercluster:

- a supercluster formed by a single cluster (i.e. without observed bremsstrahlung sub-cluster),
- a ratio $E/p > 0.9$,
- a measured brem fraction $f_{brem} < 0.5$;

big brem , or electrons with high bremsstrahlung fraction but without evidence of energy loss effects:

- a supercluster formed by a single cluster,
- a ratio $E/p > 0.9$,
- a measured bremsstrahlung fraction $f_{brem} > 0.5$;

showering , or electrons with energy pattern highly affected by bremsstrahlung losses:

- a super-cluster formed by a single cluster not falling in the "golden" or "big brem" classes, or a super-cluster formed by several sub-clusters.

In addition, "crack" electrons are defined as electrons whose supercluster's starting crystal is close to an η boundary between ECAL barrel modules, or close to an η boundary between the ECAL barrel and ECAL endcaps. The population of electrons in the different classes is shown in Fig. 6 as a function of the generated η for electrons with a uniform p_T distribution between 2 and 150 GeV/c . The shape of the distribution for the showering class clearly reflects the η distribution of the material thickness. The integrated fractions of reconstructed electrons in the different classes are as follows: 29.8% (golden), 12.2% (big brem), 53.3% (showering) and 4.7% (cracks).

In order to obtain a highest accuracy in momenta determination and also gain in the performance of the reconstruction algorithm this classification should be improved and extended considering the particle-flow approach.

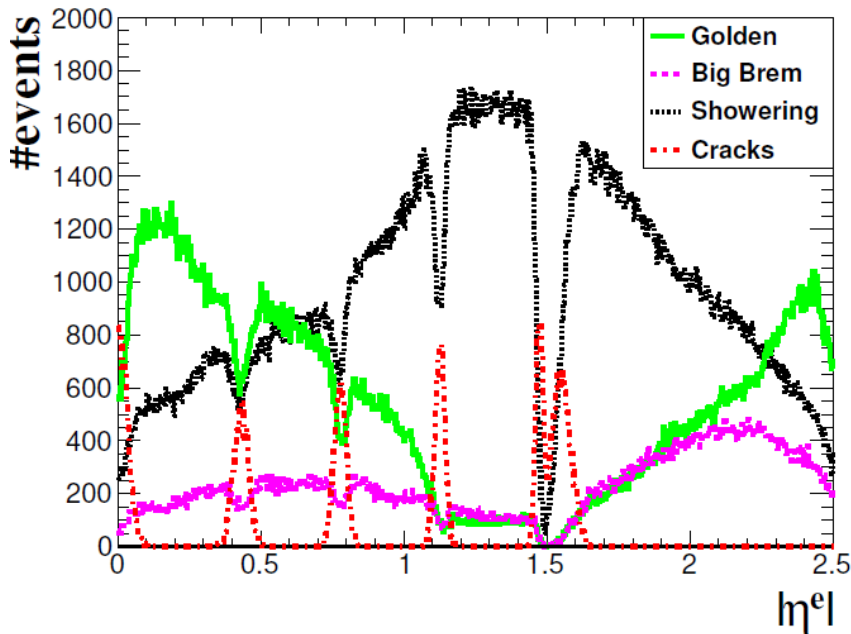


Figure 6: The electron population in the different classes as a function of the generated pseudorapidity for dielectrons with an initial transverse momentum uniformly distributed between 2 and 150 GeV/c .

In order to combine the ECAL and tracker estimates, it is useful to analyze both measurement performance as a function of a variable sensitive to the amount of bremsstrahlung radiation. Fig. 7 presents the ratios E/E_e and p/E_e as a function of E/p for the barrel case, where E stands for the super-cluster corrected energy and p is the track momentum at the innermost track position using the mode estimate. A similar behavior is found for the endcaps.

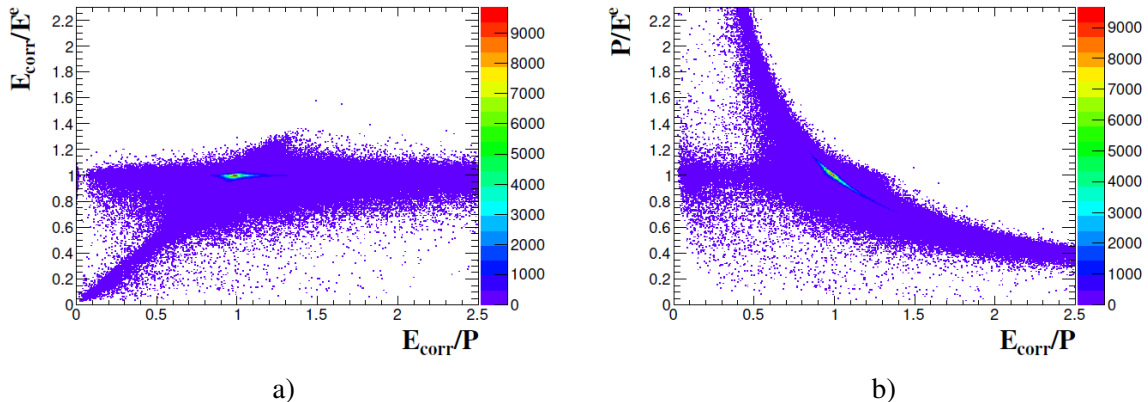


Figure 7: The momentum estimate from the ECAL and the tracker as a function of E/p for electrons in the ECAL barrel: a) supercluster energy normalized to the initial electron energy as a function of E/p ; b) reconstructed track momentum normalized to the initial electron energy as a function of E/p .

From these correlations one can identify three main regions:

- cases with $E/p \sim 1$ where both the energy and momentum estimates are in good agreement with the generated value,
- cases with $E/p > 1$ where the tracker momentum measurement is always underestimated,
- cases with $E/p < 1$ where either the ECAL or the tracker measurement can be incorrect. Most of these cases correspond to showering electrons.

As can be expected, the tracker measurement is more used at low energies as well as in the regions where the precision of the ECAL measurement is poor. The performances of the combined electron momentum are illustrated in Fig. 18 which presents the normalized momentum effective RMS of the combined estimate as well as of the ECAL and tracker measurements alone for electrons in the ECAL barrel. Electrons are from a sample of dielectron events with uniformly distributed transverse momentum between 2 and 150 GeV/c . The precision is clearly improved by using the combined estimate with respect to the ECAL only measurement for energies below $\simeq 25 - 30 GeV$. The normalized effective transverse momentum resolution for electrons in the ECAL barrel and electrons in the ECAL endcaps is also shown in Fig. 8.

5 Discussion and Perspectives

Electron reconstruction at the CMS experiment is performed using two complementary methods. The ECAL driven seeding algorithm, based on the matching of tracker seeds with reconstructed super-clusters provides an efficient filtering of the background from jets faking electrons. It is complemented by a tracker driven seeding, which allows to further improve the efficiency at low p_T^e and in the ECAL crack regions. Overall, the seeding efficiency for isolated electrons is $\simeq 95\%$ for $p_T^e = 10 GeV/c$ and close to 100% for $p_T^e = 100 GeV/c$. A dedicated tracking and fitting is used for electrons to better cope with the large amount of radiative energy loss in the tracker material. The trajectory building strategy allows for an efficient collection of hits up to the ECAL despite important change of curvature undergone by electrons emitting bremsstrahlung photons. The mode estimates are used in the evaluation of the track momentum parameters. A loose preselection is applied on electron candidates which allows to keep a very high efficiency while rejecting a significant part of the background.

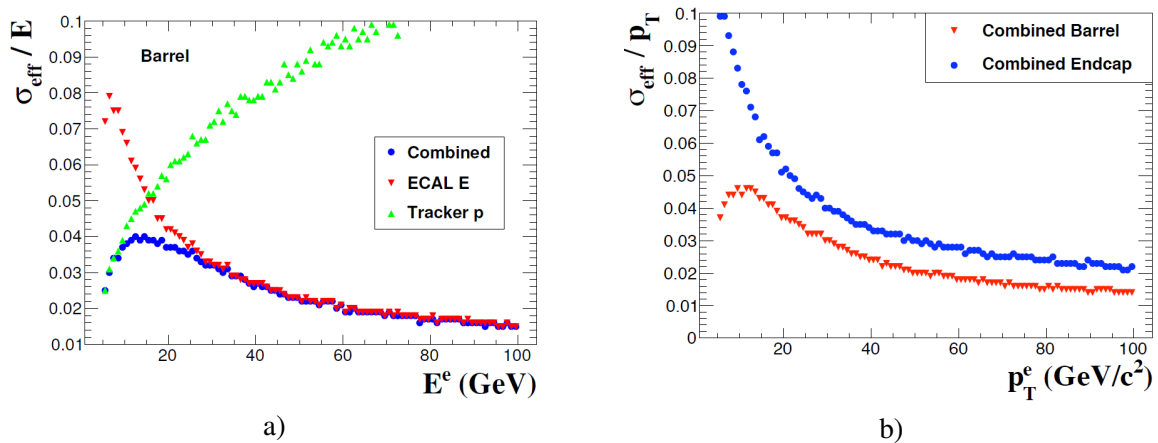


Figure 8: Performances of the combined momentum estimate: a) effective momentum resolution for the ECAL, the tracker and the combined momentum estimates as a function of the electron generated energy for electrons in the ECAL barrel and b) effective transverse momentum resolution for electrons in the ECAL barrel and electrons in the ECAL endcaps. Electrons are from a sample of di-electron events with uniformly distributed transverse momentum between 2 and 150 GeV/c .

The electron identification and reconstruction within the particle-flow algorithm consists in two main parts: a tracker-driven seeding for GSF tracks focused on low- p_T or non-isolated electrons, complementing the ECAL-driven seeding; and an electron reconstruction and identification included in the core of the particle flow algorithm. The key step of the reconstruction is the Bremsstrahlung recovery. The super-cluster thus obtained allows calorimeter-track matching variables to be easily built. The resulting observables are combined with the electron track properties in a multivariate analysis.

The reconstruction efficiency on isolated electrons is $\simeq 90\%$ for $p_T^e = 15 GeV/c$ and $\simeq 95\%$ for $p_T^e = 100 GeV/c$. The final electron momentum is based on the combination of the ECAL and tracker measurements. ECAL super-clusters errors as well as errors from the track fit are used in a weighted mean when the two measurements are in agreement. In the other cases, either the E measurement or the p measurement is used, depending on electron classes. An effective resolution of $\simeq 1\%$ is obtained for golden electrons of $E^e = 100 GeV$ in the ECAL barrel.

The discovery of the Higgs boson in the channel $H \rightarrow ZZ^* \rightarrow 4l$ and subsequent analysis of its properties requires a very accurate characterization of electrons in the detector. This is primarily due to the fact that low-mass Higgs boson is a narrow resonance. Therefore, a large error in the determination of electrons momenta for the low- p_T electrons leads to smearing of the peak of the invariant mass distribution and to deterioration of the signal to noise ratio. Also, in view of the fact that the cross-section of the Higgs boson production and decay to 4-lepton final state is small, it is needed to get the highest possible efficiency of detection of leptons in the final states, including crack-electrons.

As is evident from the written above, various algorithms for reconstruction of electron tracks have different efficiency in different parts of the spectrum. It is therefore necessary to use a combination of all available methods of reconstruction in the best way. Various algorithms can complement each other and give significant rise in the accuracy of the determination of the electron's characteristics. This combination implies to revisit the classification of the electrons taking into account the particle-flow algorithm. This task includes the review of eligibility criteria for existing classes, as well as possibly adding new ones.

The purpose of the pre-thesis internship is to improve the resolution of the transverse momentum for low- p_T electrons and crack electrons and improve E-p combination for the measured momentum and energy. This should enable better definition the characteristics of signals and improve cutting the background processes. Improved reconstruction algorithm will be applied to the analysis of 2011 experimental data from the LHC.

During the thesis work I will analyze data for the search of the Higgs boson with 4-lepton final state using improved algorithm of the leptonic final states reconstruction. This includes both work on the improvement of reconstruction algorithms and its application on the data analysis looking for an excess

of the data above the background and investigate the Higgs hypothesis and its properties.

References

- [1] P. W. Higgs, Phys. Lett. 12 (1964) 132;
- [2] F. Englert and R. Brout Phys.Rev.Lett. 13 321 (1964);
- [3] G. 't Hooft, Nuclear Phys. B 33 (1971) 173;
- [4] LHC Higgs Cross Section Working Group, S. Dittmaier, C. Mariotti, G. Passarino, and R. Tanaka (Eds.), *Handbook of LHC Higgs Cross Sections: 1. Inclusive Observables*, CERN-2011-002 (CERN, Geneva, 2011), arXiv:1101.0593 [hep-ph];
- [5] LEP Collaborations ALEPH, DELPHI, L3, OPAL, the LEP Electroweak Working Group and the SLD Heavy Flavour Group, A combination of preliminary electroweak measurements and constraints on the Standard Model, CERN-EP/2002-091, hep-ex/0212036;
- [6] arXiv:1103.3233 [hep-ph];
- [7] CERN-LHCC-2006-001;
- [8] W. Adam, R. Fruhwirth, A. Strandlie, T. Todorov, "Reconstructions of Electrons with the Gaussian-Sum Filter in the CMS Tracker at the LHC", Journal of Physics G: Nuclear and Particle Physics 31 (2005) N9. doi:10.1088/0954-3899/31/9/N01;
- [9] M. Pioppi, "Iterative tracking", CMS Internal Note IN 2007/065 (2007);
- [10] F. Beaudette, D. Benedetti, P. Janot, M. Pioppi, "Electron Reconstruction within the Particle Flow Algorithm", CMS AN -2010/034;
- [11] S. Baffioni et al., "Electron reconstruction in CMS", Eur. Phys. J. C 49 (2007) 1099;